

Hidden vibrational bistability revealed by intrinsic fluctuations of a carbon nanotube

P. Belardinelli,[†] W. Yang,[‡] A. Bachtold,^{*,‡} M.I. Dykman,^{*,¶} and F. Alijani^{*,§}

[†]*Department of Construction, Civil Engineering and Architecture, Polytechnic University of Marche, 60131 Ancona, Italy*

[‡]*ICFO - Institut de Ciències Fòniques, The Barcelona Institute of Science and Technology, 08860 Castelldefels, Barcelona, Spain*

[¶]*Department of Physics and Astronomy, Michigan State University, East Lansing, MI 48824, USA*

[§]*Department of Precision and Microsystems Engineering, Delft University of Technology, Mekelweg 2, 2628CD, Delft*

E-mail: Adrian.Bachtold@icfo.eu; dykmanm@msu.edu; f.aliyani@tudelft.nl

Abstract

We demonstrate that a quiet state and large-amplitude self-sustained oscillations can co-exist in a carbon nanotube subject to time-independent drive. A feature of the bistability is that it would be hysteresis-free in the absence of noise and the oscillatory state would not be seen. It is revealed by random switching between the stable states, which we observe in the time domain. We attribute the switching to fluctuations in the system and show that it displays Poisson statistics. We propose a minimalistic model that relates the emergence of the bistability to a non-monotonic variation of nonlinear friction with the vibration amplitude. This new type of dynamical regime and the means to reveal it are generic and are of interest for various mesoscopic vibrational systems.

Keywords: carbon nanotube, self-oscillations, hysteresis-free bistability, stochastic switching, nonlinear friction

Nano-electro-mechanical systems (NEMS) provide a means for studying physics away from thermal equilibrium in a well-characterized setting.¹ An important group of non-equilibrium phenomena originates from the interplay between nonlinearity and fluctuations in driven systems, which can modify the frequency stability,²⁻⁶ the power spectrum,^{7,8} lead to spectral broadening⁹, and thermal noise squeezing.^{8,10,11} The interplay is most nontrivial when a non-equilibrium system is brought into a regime where it exhibits bistability. Here, fluctuations, even if weak on average, can cause interstate transitions and are ultimately responsible for the distribution of a system over the stable states.¹ Much work on studying these effects and the emerging scaling^{12,13} has been carried out on nano- and micromechanical resonators driven by an external resonant force or modulated parametrically.^{7,14-23} A mechanism that leads to the onset of bistability in NEMS without periodic driving was suggested in Ref.²⁴ and such bistability was observed in a carbon nanotube (CNT).²⁵

In almost all bistable mesoscopic vibrational systems, the vibrations could be brought to one of the stable states by smoothly changing a control parameter, for example, the driving force. As a result of the change, at some critical parameter value, the bifurcation point, one of the stable states would lose stability, and the system would switch to another stable state. Such behavior is usually accompanied by hysteresis: in a parameter range between bifurcation points the state of the system depends on the history of the parameter change. In all works on NEMS thus far hysteresis was used to reveal the bistability.

In this paper, we report the observation of a hysteresis-free bistability in a nanomechanical system. Such bistability means that, as the the control parameter is changed back and forth, the system remains in the quiet state. The very presence of another stable state is revealed by fluctuations that cause interstate transitions. In our system, coexisting are the quiet state and the state of large-amplitude self-sustained oscillations of the lowest mode of a CNT driven by a time-independent source-drain voltage, see Fig. 1. The large-amplitude

oscillatory state was already identified in Ref.²⁶ It is important that the mode experiences fluctuations. We reveal that the system is actually bistable by examining the fluctuation statistics. In distinction from the more conventional scenario, the large-amplitude oscillatory state emerges as the source-drain voltage is increased, and when it emerges, it is already well separated from the quiet state in phase space. Then, as the source-drain voltage is further changed, the vibrational state is observed to lose stability. There is no hysteresis when the bifurcation parameter is moved back and forth. In terms of the bifurcation theory,²⁷ the emerging and disappearing stable states are associated with an “isola”: an isolated branch of an equilibrium state of a noise-free system.

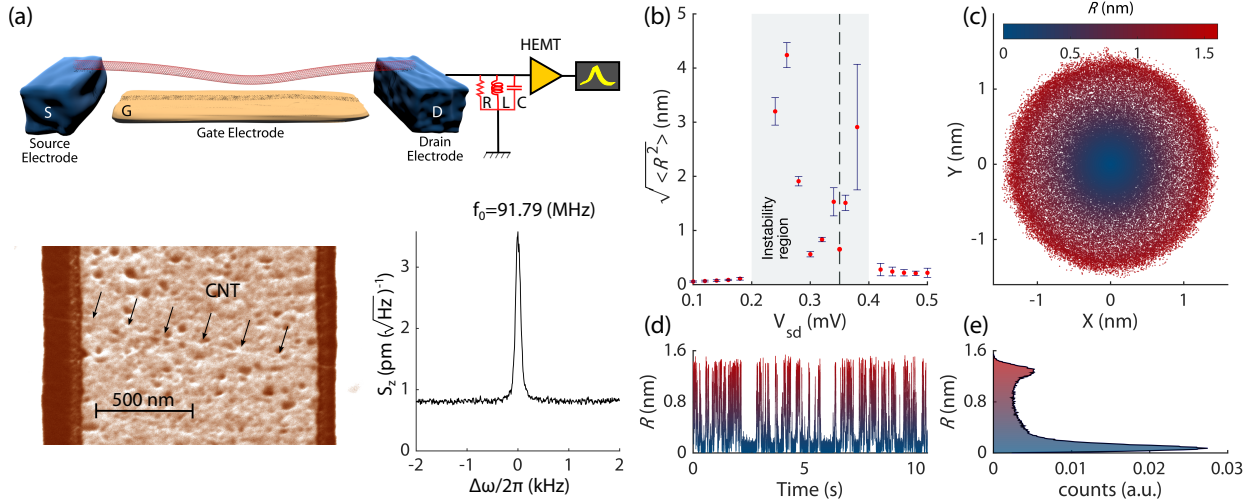


Figure 1: (a) CNT-based electromechanical oscillator and measurement schematic. The CNT has the length of $\approx 1.5 \mu\text{m}$ and the radius of $\approx 1 \text{ nm}$ (scanning electron microscope image in the bottom left panel). Voltages V_{sd} and V_{g} are applied to electrodes S and Gate, respectively. The drain electrode D is connected to an RLC resonator ($f_{\text{RLC}}=1.27 \text{ MHz}$). The displacement spectral density is shown in the bottom right panel. (b) The root mean square nanotube displacement from the origin $\sqrt{\langle R^2 \rangle}$ as a function of the source-drain voltage V_{sd} for $V_{\text{g}} = -616 \text{ mV}$; $\sqrt{\langle R^2 \rangle}$ is obtained from spectral noise measurements for all the data points except for $V_{\text{sd}} = 0.35 \text{ mV}$ (dashed line), the latter is obtained by recording the time evolution of the displacement amplitude at the mode antinode. (c) The measured two quadratures X and Y of the motion on the (X, Y)-plane at this V_{sd} , (d) fluctuations of the amplitude $R = \sqrt{X^2 + Y^2}$ in time for the same V_{sd} , (e) the amplitude histogram, normalized with respect to the total number of observations.

The experiment is done using clamped-clamped CNTs grown by chemical vapour deposi-

tion across two metallic contact electrodes.²⁸ The measurements are performed at cryogenic temperature (70mK) by applying a voltage bias to the source (V_{sd}) and to the gate electrode (V_g) which is placed beneath the CNT. The current from the drain electrode is measured by using a RLC resonant circuit and a low-temperature HEMT amplifier, see Fig. 1(a). The read-out signal is obtained by measuring the current noise spectrum, which is converted to the nanotube displacement.²⁶ The same calibration is used to obtain the quadratures of the motion (X,Y) from the lock-in measurements. The scaled vibration amplitude is $R = \sqrt{X^2 + Y^2}$.

When sweeping up the source-drain voltage V_{sd} at $V_g = -616$ mV, there occurs a sudden jump up in the displacement R for $V_{sd} \approx 0.2$ mV followed by a jump down at $V_{sd} \approx 0.4$ mV, see highlighted region of Fig. 1(b). The change of the nanotube motion with V_{sd} in Fig. 1(b) does not resemble that of a vibrational system undergoing a supercritical Hopf bifurcation, whose signature is a smooth monotonic increment of the oscillation amplitude and loss of stability of the quiet state.²⁹ The instability is observed over a narrow range of gate voltage V_g but reappears periodically in V_g with a period corresponding to adding four electrons to the nanotube. The periodicity is consistent with the SU(4) symmetry of the CNT.²⁶

In the (X,Y) space at $V_{sd} = 0.35$ mV we recognize a highly populated doughnut-like region centered at a nonzero mean amplitude that encircles the thermal motion about the origin of the quadrature space. This region suggests the presence of an oscillatory state, see Fig. 1(c). The time trace of the motion (Fig. 1(d)) and the normalized histogram of the amplitude R in Fig. 1(e) further support the notion that the system has two different dynamical states. While distinct peaks in the amplitude distribution may serve as a signature of co-existing states, a double-peak pattern can also arise in various other dynamical phenomena such as intermittent chaos or bursting oscillations.³⁰ A careful analysis is required to differentiate bistability from aperiodic dynamical behaviors.

To understand the nature of the observed dynamics, we perform statistical analysis on the time-domain data of Fig. 1(d). This dataset has not been presented in the earlier work.²⁶ We

assume that our system has two stable states, namely a zero-amplitude, i.e. a quiet state, and a self-sustained oscillatory state, which has a large amplitude compared to the root-mean-square amplitude fluctuations³¹⁻³⁴. We investigate whether noise induces stochastic transitions between the stable states, analogous to the noise-induced interwell hopping of a damped particle in a double-well potential, see Fig. 2(a), cf.³⁵; such hopping underlies stochastic resonance.^{36,37} The difference in our case is that here one of the stable states is a static equilibrium point, whereas the other is a state of self-sustained vibrations.

Noise-induced switching is well-defined if the switching rate is much smaller than the relaxation rate. A noise-driven system then spends most of the time fluctuating about one of its stable states. The characteristic correlation time t_r of these fluctuations is the dynamical relaxation time or the correlation time of the noise. Occasionally there occur large outbursts of noise that lead to switching between the states. The typical time between such outbursts is much larger than t_r , whereas the duration of the switching event itself is comparable to t_r . Therefore the switching events are expected to be uncorrelated and described by the Poissonian statistics.

In order to detect interstate switching events, one would need to set a threshold, which is related to but does not coincide with the basin boundary of the two states. For a particle in a double-well potential, reaching the barrier top does not necessarily lead to switching, as the system can go back to the initially occupied well. Even in the simplest case of fluctuations induced by white noise, to find the switching rate one has to set up a threshold sufficiently far beyond the barrier top with respect to the initially occupied state, as has been known since the classical work of Kramers.³⁸ It is clear from the above arguments that the thresholds for transitions between different states should not coincide, cf.³⁹ Hence, we introduce two amplitude thresholds, R_L and R_H , see Fig. 2(a). If the system was fluctuating about $R = 0$ and its trajectory crossed R_H , we assume that it has switched to the large-amplitude state. On the other hand, if the system was fluctuating about the large-amplitude state and its trajectory $R(t)$ crossed R_L , it has switched to the $R = 0$ -state. With the above definition,

the dwell (residence) times τ_{up} and τ_{down} are the times spent in the zero- and large-amplitude states, respectively, before the system switches. The time intervals τ_{up} and τ_{down} are shown in Fig 2(b) by the red and blue thick bars, respectively. The region between R_H and R_L contains the separatrix. The experimental data do not allow us to find it.

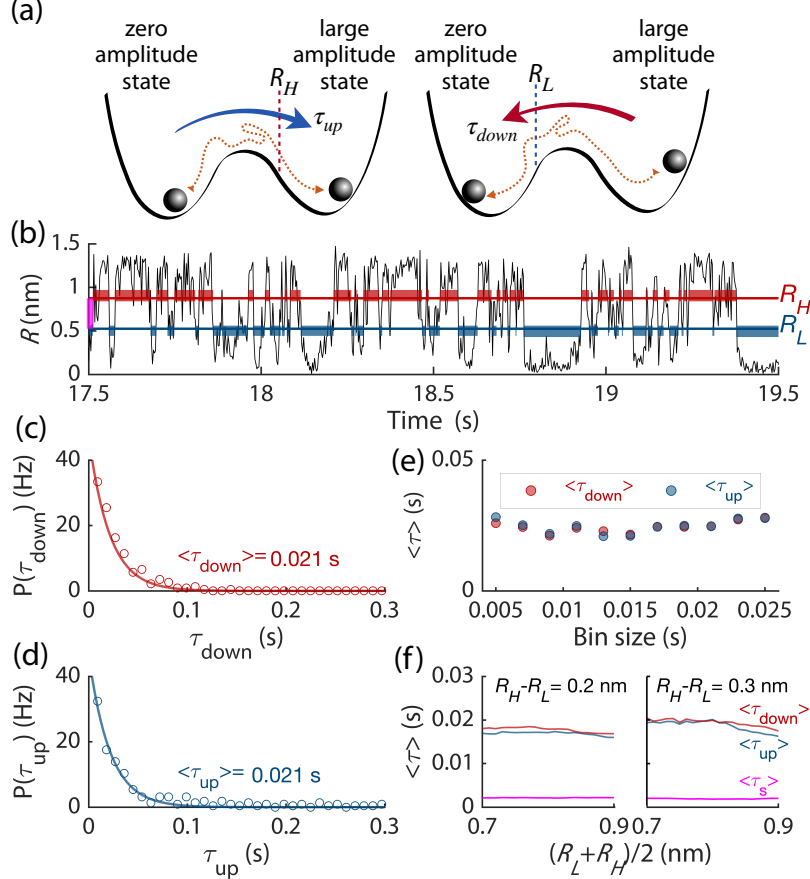


Figure 2: (a) A double-well potential, illustrating bistable dynamics using a ball-in-a-cup analogy. The minima are associated with the stable state of self-sustained vibrations and the zero-amplitude state of the CNT. Noise-induced transitions to the large-amplitude (zero-amplitude) states are considered to occur once the vibration amplitude crosses the threshold R_H (R_L). (b) A sample of the time evolution of the vibration amplitude ($V_{\text{sd}} = 0.35$ mV). Blue/red bars indicate the chosen switching thresholds with $R_H - R_L = 0.35$ nm, $(R_H + R_L)/2 = 0.7$ nm. The magenta bar indicates the region between R_H and R_L . (c)-(d) Dwell (residence) time distributions (bin size 9 ms) for the large-amplitude state [panel (c)] and the zero-amplitude state [panel (d)]. A Poisson distribution (Eq. (1)) is fitted to the data. It gives averaged dwell times of $\langle \tau_{\text{down}} \rangle = 0.021$ s and $\langle \tau_{\text{up}} \rangle = 0.021$ s. (e) Influence of the bin size on the average dwell times in panels c and d. (f) Average dwell times for varying thresholds R_L and R_H . The average time $\langle \tau_s \rangle$ is the time spent in between the two thresholds.

Figures 2(c) and 2(d) show the distribution of the dwell times τ_{up} and τ_{down} . The transitions between the states are well described by a Poisson process, and the distribution of the dwell times is close to exponential,

$$P(\tau) = \frac{1}{\langle \tau \rangle} e^{-\tau/\langle \tau \rangle}. \quad (1)$$

This is the central argument in support of the coexistence of two stable states in our system. We use Eq. (1) to fit the experimental data and find that the dwell times are approximately the same for the chosen parameters, with $\tau_{\text{up}} \approx \tau_{\text{down}} \approx 21$ ms. The fit is only mildly influenced by the bin size, see Fig. 2(e). These dwell times are much larger than the relaxation time t_r of the nanotube, which can be inferred from duration of the switching events themselves: in Fig. 2(b) the trajectories leading to transitions are essentially vertical. The detailed data indicates that $t_r \sim 1$ -3 ms, as illustrated in Fig. 2(f) by the average time $\langle \tau_s \rangle$ spent in between the two thresholds.

Another important argument in support of the bistability is seen from Fig. 2(f). In this figure we plot the dwell times over a broad range of mean threshold values and separations. The results do not change. This demonstrates the reliability and stability of the two-threshold approach and confirms the presence of noise-induced hopping between two metastable states. The stochastic analysis conducted on an additional temporal dataset, corresponding to $V_{\text{sd}} = 0.25$ mV, also aligns with these findings (see Supporting Information S1⁴⁰).

The bistable dynamics observed in Fig. 2 ultimately comes from the source-drain voltage V_{sd} , which pumps energy into the system. The onset of self-sustained vibrations due to energy pumping is often associated with the friction coefficient becoming negative, which makes the quiet state unstable. In contrast, in our system the quiet state remains stable. This can be understood if the friction coefficient becomes negative in a certain range of sufficiently large vibration amplitude. The dependence of the friction coefficient on amplitude is called

nonlinear friction. Such friction is well-known in nanomechanics.^{1,41} Usually it leads to a faster decay of vibrations with the increasing amplitude, that is, the coefficient of nonlinear friction is positive, although there has been also observed slowing down of the decay with the increasing amplitude.⁴²

There are several possible causes of nonlinear friction in our system. One of them is the electron-vibrational coupling. As electrons hop between the leads and the nanoresonator, they exchange energy with the mode. This leads to decay or excitation of the vibrations, i.e., to positive or negative friction, see^{24,43–47} and references therein. The analyses in these papers refer to the limit of strong Coulomb blockade. Negative nonlinear friction resulted from the dependence of the tunneling on the vibration amplitude.^{24,45} This dependence should occur in our system, too, even though the Coulomb gap is moderately hard. One can picture this dependence as coming from the change of the transmission of the tunneling barrier due to the strain induced by the CNT displacement.⁴⁸

In the basic model of the effect of vibrations on tunneling⁴⁹ the vibration-induced change of the tunneling exponent is $C_{\text{tun}}q/\lambda_{\text{tun}}$, where q is the mode coordinate and λ_{tun} is the electron tunneling length. In the measurements presented in this work, the tunnel barriers are defined in the clamping areas at the interface between the nanotube and the metal electrodes. For tunneling onto/from a CNT, the coefficient C_{tun} depends on the structure of this interface, which is not well characterized, and therefore it cannot be found quantitatively. However, the ratio q/λ_{tun} itself is $\gtrsim 10$ for the observed limit cycle radius and $\lambda_{\text{tun}} \sim 3-4 \text{ \AA}$. This suggests that the friction that results from the modulation of the tunneling barrier can be significantly nonlinear. It can be negative in the range of V_{sd} where the energy transfer to the mode exceeds the energy drain from the mode. The amplitude dependence of the friction is affected also by the polaronic effect: because of the gate voltage, electrons exert force on the mode that depends on the number of electrons on the CNT, which itself depends on the CNT displacement. This force leads to vibration decay, for strong Coulomb blockade.⁴⁶

Another source of negative nonlinear friction, a retarded backaction from the circuit,

is discussed in the SI Sec. S2.⁴⁰ Here, a quantitative theory requires the knowledge of the nonlinear dependence of the conductance on the vibration amplitude, which itself requires full characterization of the clamping area. However, the magnitude of this nonlinear friction force compared to the linear one is proportional to the square of the ratio of the displacement amplitude to the distance to the gate electrode and thus relatively small.

The above arguments show that the situation with nonlinear friction is no different from linear friction, which comes from several possible mechanisms. Therefore, to describe the central experimental observation, the onset and collapse of self-sustained vibrations, we use a minimalistic model. A major feature of this model is the absence of delay in the friction force, in the rotating frame. This is a consequence of the smoothness of the density of states of the electrons and thermal acoustic phonons involved in the mode decay processes, cf.¹

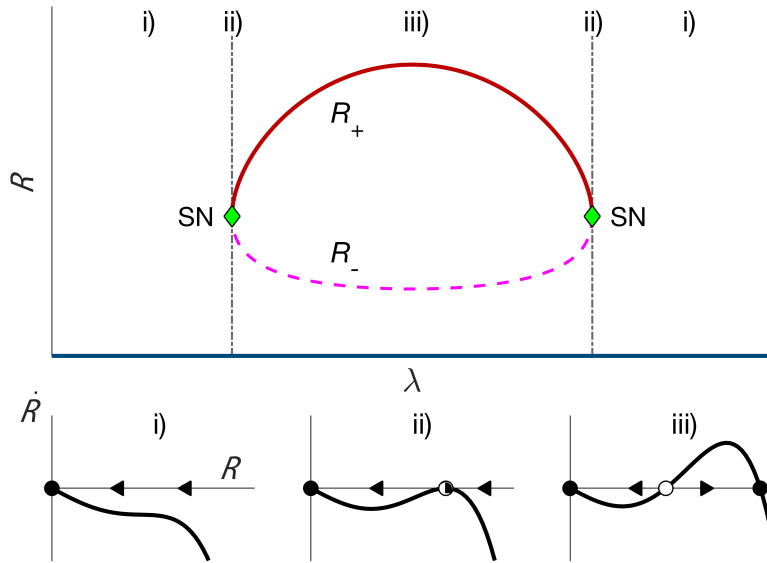


Figure 3: Upper panel: Steady-state solutions as a function of the bifurcation parameter λ . In our nanomechanical resonator λ is a function of V_{sd} . Solid/dashed lines are stable (R_+)/unstable (R_-) solution branches. The isola emerges as a result of non-monotonic nonlinear damping. Lower panel: sketches of the phase portrait of the vibration radius. (i) The radial phase portrait for λ below and above the isola bifurcation point. The solid dot is a stable solution. (ii) The saddle-node bifurcation (SN) at a finite vibration radius, indicating the onset of an isola. (iii) Bistable region with co-existing zero and large amplitude states. The open circle is an unstable solution, which corresponds to an unstable limit cycle. The arrows in panels (i), (ii), and (iii) indicate the dynamical flow.

Since the vibration frequency is much higher than all other rates and frequencies in the system, the vibrations can be described in the rotating frame using a complex vibration amplitude $z(t) = C_z[q + i(p/m\omega_0)] \exp(i\omega_0 t)$, where q and p are the mode coordinate and momentum, m is its effective mass, ω_0 is the eigenfrequency and C_z is a scaling parameter. In the rotating wave approximation (RWA) the equation of motion (see Sec. S3 of the Supporting Information⁴⁰) reads

$$\dot{z} = - [\Gamma + (\gamma_{\text{nlf}} - i\gamma_D)|z|^2 + |z|^4] z. \quad (2)$$

Here Γ and γ_{nlf} are the coefficients of linear and nonlinear friction, whereas γ_D is the Duffing nonlinearity. The RWA applies provided $|\dot{z}| \ll \omega_0|z|$. The right-hand side of Eq. (2) is our minimalistic model of nonlinear friction: it is an expansion in z , valid when the vibration amplitude is comparatively small, so that the decay rate and the change of the vibration frequency are $\ll \omega_0$. The term $\propto |z|^4 z$ describes quintic nonlinear friction, cf.⁵⁰ It must be taken into account where the conventional friction coefficients Γ and γ_{nlf} become small. A simple microscopic model of such friction is provided in Supporting Information S4.⁴⁰ In distinction from the conventional analysis of the onset of self-oscillations, which uses the model (2) without the quintic term, to describe the experiment we have to assume that the parameter Γ remains positive, and it is γ_{nlf} that is the bifurcation parameter that changes sign.

We rewrite Eq. (2) in polar coordinates by setting $z(t) = R(t)e^{i\theta(t)}$, where R and θ are the vibration amplitude and the “slow” part of the vibration phase. From Eq. (2)

$$\dot{R} = -f_{\text{nlf}}R, \quad \dot{\theta} = \gamma_D R^2, \quad (3)$$

with the coefficient of nonlinear friction being

$$f_{\text{nlf}} = \Gamma + \gamma_{\text{nlf}}R^2 + R^4. \quad (4)$$

For $\Gamma > 0$ the quiet state $R = 0$ is stable. If Γ becomes negative, the state $R = 0$ becomes unstable, and for $\gamma_{\text{nlf}} > 0$ there emerges a stable limit cycle with radius $\propto (|\Gamma|/\gamma_{\text{nlf}})^{1/2}$ (supercritical Hopf bifurcation). If Γ is positive but γ_{nlf} becomes negative, there emerges an unstable limit cycle with radius $(\Gamma/|\gamma_{\text{nlf}}|)^{1/2}$ (subcritical Hopf bifurcation).

The term R^4 in f_{nlf} leads to the onset of a stable limit cycle for $\gamma_{\text{nlf}} < 0$ and $\Gamma > 0$ along with an unstable one. The radii of the cycles as given by the condition $f_{\text{nlf}} = 0$ are

$$R_{\pm} = \frac{1}{\sqrt{2}} \left[-\gamma_{\text{nlf}} \pm \sqrt{\gamma_{\text{nlf}}^2 - 4\Gamma} \right]^{1/2} \quad (5)$$

For $-\gamma_{\text{nlf}} > 2\Gamma^{1/2}$ the cycle with the radius R_+ is stable, whereas the cycle with the radius R_- is unstable. At $\gamma_{\text{nlf}} = -2\Gamma^{1/2}$ the two cycles merge and annihilate one another in a saddle-node bifurcation. For smaller $|\gamma_{\text{nlf}}|/2\Gamma^{1/2}$ they disappear.

We now relate model (2) to the experiment. The values of Γ and γ_{nlf} change with the control parameter V_{sd} . In particular, Γ decreases as we approach the bistability region in Fig. 1(b).²⁶ The key observations are: (i) a stable zero-amplitude state and a stable limit cycle co-exist in a certain parameter range, (ii) the zero-amplitude state is stable not only outside, but also inside this range, and (iii) the limit cycle is excited and collapses with the varying parameters while still having a large amplitude. This scenario is qualitatively different from the standard subcritical Hopf bifurcation that is accompanied by hysteresis.

A minimalistic picture that describes the experiment is that, as the source-drain voltage V_{sd} varies, there first occurs a saddle-node bifurcation at $-\gamma_{\text{nlf}} = 2\Gamma^{1/2}$. At this bifurcation there emerge the stable and unstable limit cycle with amplitudes R_{\pm} . As V_{sd} varies further, these limit cycles merge together and disappear via another saddle-node bifurcation. This is illustrated in Fig. 3.

To link the above phenomenology to Eqs. (3) and (4) we should consider how the parameters of these equations depend on V_{sd} . A major factor is the V_{sd} -dependence of γ_{nlf} , since this parameter becomes negative and, moreover, exceeds $2\Gamma^{1/2}$ in the absolute value.

It should be noted that the linear friction coefficient Γ also depends on V_{sd} , as reported in.²⁶ Overall, γ_{nlf} should be non-monotonic as a function of V_{sd} to allow for both the onset and the disappearance of the bistability with the increasing V_{sd} . The analysis simplifies for the gate voltage V_g where the range of V_{sd} in which the zero-amplitude state co-exists with the vibrational state is narrow. In this case one can approximate

$$\gamma_{\text{nlf}}(V_{\text{sd}}) + 2\sqrt{\Gamma(V_{\text{sd}})} = -\eta(V_B^{(1)} - V_{\text{sd}})(V_{\text{sd}} - V_B^{(2)}) \quad (6)$$

Here, the parameter $\eta > 0$ is a scaling parameter and $V_B^{(1,2)}$ are the bifurcational values of V_{sd} . The CNT shows bistability in the range $V_B^{(2)} < V_{\text{sd}} < V_B^{(1)}$.

The quadratic dependence of γ_{nlf} and the corresponding dependence of R_+ on V_{sd} provide an insight into our observations, but do not fully describe the evolution of the dynamics within the instability region. The complicated dependence of R_+ on V_{sd} can have several causes, including defects in the CNT that lead to a nonuniform electron density, as well as the interplay of the Kondo effect and the Coulomb blockade, which depend on the bias and the gate voltage, thus modifying the tunneling and the polaronic effect and ultimately the friction force. In Fig. 4 we show that the complex behavior of the vibration amplitude within the instability region can be effectively captured by considering a non-monotonic dependence of the nonlinear friction force on the source-drain voltage. Given that the dependence of the root mean square vibration amplitude $\langle R^2 \rangle^{1/2}$ on V_{sd} in Fig. 1(b) resembles an inverted quartic parabola, we describe the dynamics within the bistability region by a constant linear friction and a 5-parameter nonlinear friction, $\gamma_{\text{nlf}} = \sum_{n=0}^4 (\gamma_n V_{\text{sd}}^n)$. To numerically obtain the parameters that match the experiment we positioned the saddle-node points of the isola at the boundaries of the instability region observed experimentally and constrained the amplitude of the self-oscillations to match the measured $\sqrt{\langle R^2 \rangle}$ values.

We plot in Fig. 4(a) the evolution of the amplitude variance as a function of V_{sd} by simulating the stochastic dynamics of Eq. (2) in the quadrature space, in which each quadrature

is affected by an independent random Wiener process (See Sec. S5 of the Supporting Information⁴⁰ for more details). The noise, which is white in the slow time $\sim \Gamma^{-1}$, $(|\gamma_{\text{nlf}}| \langle R^2 \rangle)^{-1}$, comes from different intrinsic sources, such as hopping of the electrons on and off the CNT and creation and annihilation of thermal phonons nonlinearly coupled to the mode. In the phase-space of the two quadratures (X, Y) the trajectories fluctuate about a circle with radius $\langle R^2 \rangle^{1/2}$ or about the quiet state $R = 0$, switching between them, see Fig. 4(b) and (c). Respectively, the stationary probability distribution of $R(t)$ displays two peaks, as seen in Fig. 4(d).

We emphasize that the non-monotonic dependence of the nonlinear friction parameter γ_{nlf} on V_{sd} , with γ_{nlf} being negative in a certain range of V_{sd} , is critical for the emergence of the isola and the hysteresis-free bistability. At the same time, fluctuations in the system are crucial for revealing the bistability.

Although isolas in multistable systems have attracted much attention theoretically,^{51–54} their experimental demonstrations have almost exclusively been limited to macroscale systems under periodic driving.^{55–57} In mesoscopic systems, the only reported observation of isolas involves forced vibrations of a nonlinear microresonator with coupled vibrational modes.⁵⁸ In nanomechanics, isolas have not been observed. Here, we demonstrate the existence of an isolated vibrational state in a nanomechanical system subject to a time-independent drive. Specifically, we show that driving a carbon nanotube by a dc source-drain voltage V_{sd} leads to the onset of bistability, in which a stable quiet state coexists with periodic self-sustained vibrations. We show that the bistability is non-hysteretic: varying the control parameter would not lead to switching between the branches of the stable states. We also provide a minimalistic phenomenological model that describes the effect and indicate the mechanisms that can underlie this model.

Supporting Information: Additional analysis of the statistics of stochastic switching of the carbon nanotube, discussion on the friction force generated due to electrothermal backaction, theoretical description of the mechanism leading to quintic nonlinear friction, and more

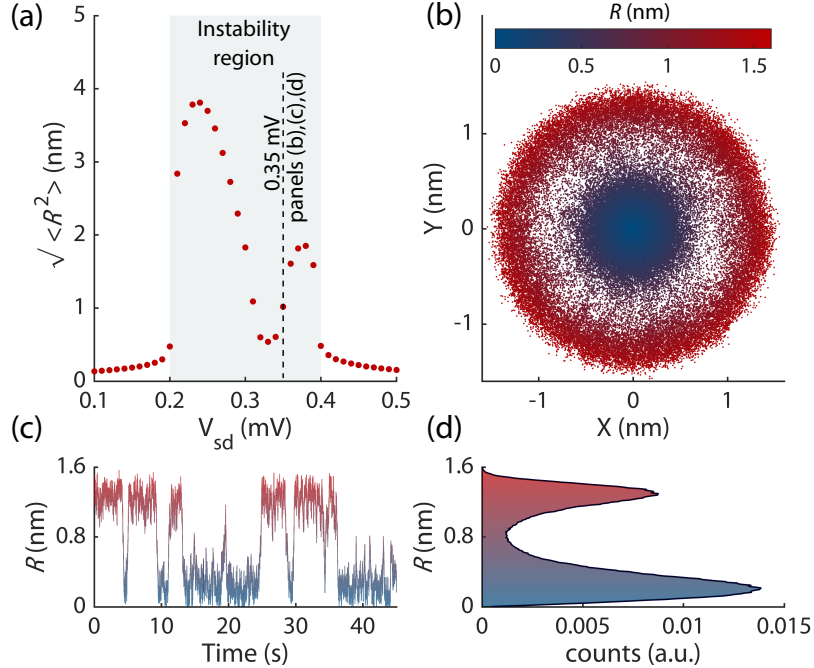


Figure 4: Numerical simulations of the fluctuation dynamics of the nanotube. (a) The standard deviation of the nanotube displacement $\sqrt{\langle R^2 \rangle}$ as a function of the source-drain voltage V_{sd} . Each point is the average of ten simulations. The stochastic dynamics is characterized for one simulation at $V_{sd} = 0.35$ mV (dashed line) in panels (b)-(d). (b) The phase space of the two quadratures of the motion (X, Y). (c) Fluctuations of the amplitude $R = \sqrt{X^2 + Y^2}$ in time. (d) The amplitude histogram of the time trace of panel (c) normalized with respect to the total number of observations. Details of the simulations of the stochastic dynamics of the nanotube are provided in Sec. S5 of the Supporting Information.⁴⁰

information on the numerical simulations.

Acknowledgement

We are grateful to Fabio Pistolesi for the discussion of the electron-phonon coupling in CNT. Financial support was provided from the European Union’s research and innovation programme under ERC starting grant no. 802093, ERC consolidator grant no. 101125458, and ERC advanced grant no. 692876. MID acknowledges partial support from the US Defense Advanced Research Projects Agency (Grant No. HR0011-23-2-004) and from the Moore Foundation (Grant No. 12214). PB acknowledges partial support from the European

Union's NextGenerationEU programme, in the framework of PRIN 2022, project DIMIN. AB acknowledges MICINN Grant No. RTI2018-097953-B-I00 and PID2021-122813OB-I00, AGAUR (Grant No. 2017SGR1664), the Fondo Europeo de Desarrollo, the Spanish Ministry of Economy and Competitiveness through Quantum CCAA, TED2021-129654B-I00, EUR2022-134050, and CEX2019-000910-S [MCIN/AEI/10.13039/501100011033], MCIN with funding from European Union NextGenerationEU (PRTR-C17.I1) and Generalitat de Catalunya, CERCA, Fundacio Cellex, Fundacio Mir-Puig.

References

- (1) Bachtold, A.; Moser, J.; Dykman, M. I. Mesoscopic Physics of Nanomechanical Systems. *Rev. Mod. Phys.* **2022**, *94*, 045005.
- (2) Greywall, D. S.; Yurke, B.; Busch, P. A.; Pargellis, A. N.; Willett, R. L. Evading amplifier noise in nonlinear oscillators. *Phys. Rev. Lett.* **1994**, *72*, 2992–2995.
- (3) Villanueva, L. G.; Kenig, E.; Karabalin, R. B.; Matheny, M. H.; Lifshitz, R.; Cross, M. C.; Roukes, M. L. Surpassing Fundamental Limits of Oscillators Using Nonlinear Resonators. *Phys. Rev. Lett.* **2013**, *110*, 177208.
- (4) Kenig, E.; Cross, M. C.; Moehlis, J.; Wiesenfeld, K. Phase Noise of Oscillators with Unsaturated Amplifiers. *Phys. Rev. E* **2013**, *88*, 062922.
- (5) Zhang, B.; Yan, Y.; Dong, X.; Dykman, M.; Chan, H. Frequency stabilization of self-sustained oscillations in a sideband-driven electromechanical resonator. *Phys. Rev. Appl.* **2024**, *22*, 034072.
- (6) Sadeghi, P.; Demir, A.; Villanueva, L. G.; Kähler, H.; Schmid, S. Frequency fluctuations in nanomechanical silicon nitride string resonators. *Phys. Rev. B* **2020**, *102*, 214106.

- (7) Stambaugh, C.; Chan, H. B. Supernarrow Spectral Peaks near a Kinetic Phase Transition in a Driven Nonlinear Micromechanical Oscillator. *Phys. Rev. Lett.* **2006**, *97*, 110602.
- (8) Huber, J. S.; Rastelli, G.; Seitner, M. J.; Kölbl, J.; Belzig, W.; Dykman, M. I.; Weig, E. M. Spectral Evidence of Squeezing of a Weakly Damped Driven Nanomechanical Mode. *Phys. Rev. X* **2020**, *10*, 021066.
- (9) Rechnitz, S.; Tabachnik, T.; Shlafman, M.; Shlafman, S.; Yaish, Y. E. Mode coupling bi-stability and spectral broadening in buckled carbon nanotube mechanical resonators. *Nature Communications* **2022**, *13*, 5900.
- (10) Buks, E.; Yurke, B. Dephasing Due to Intermode Coupling in Superconducting Stripline Resonators. *Phys. Rev. A* **2006**, *73*, 023815.
- (11) Yang, F.; Fu, M.; Bosnjak, B.; Blick, R. H.; Jiang, Y.; Scheer, E. Mechanically Modulated Sideband and Squeezing Effects of Membrane Resonators. *Phys. Rev. Lett.* **2021**, *127*, 184301.
- (12) Dykman, M.; Krivoglaz, M. Fluctuations in nonlinear systems near bifurcations corresponding to the appearance of new stable states. *Physica A: Statistical Mechanics and its Applications* **1980**, *104*, 480–494.
- (13) Dykman, M. I. Critical exponents in metastable decay via quantum activation. *Phys. Rev. E* **2007**, *75*, 011101.
- (14) Aldridge, J. S.; Cleland, A. N. Noise-Enabled Precision Measurements of a Duffing Nanomechanical Resonator. *Phys. Rev. Lett.* **2005**, *94*, 156403.
- (15) Chan, H. B.; Stambaugh, C. Activation Barrier Scaling and Crossover for Noise-Induced Switching in Micromechanical Parametric Oscillators. *Phys. Rev. Lett.* **2007**, *99*, 060601.

- (16) Karabalin, R. B.; Lifshitz, R.; Cross, M. C.; Matheny, M. H.; Masmanidis, S. C.; Roukes, M. L. Signal Amplification by Sensitive Control of Bifurcation Topology. *Phys. Rev. Lett.* **2011**, *106*, 094102.
- (17) Venstra, W. J.; Westra, H. J. R.; van der Zant, H. S. J. Stochastic Switching of Cantilever Motion. *Nat. Commun.* **2013**, *4*, 2624.
- (18) Defoort, M.; Puller, V.; Bourgeois, O.; Pistolesi, F.; Collin, E. Scaling Laws for the Bifurcation Escape Rate in a Nanomechanical Resonator. *Phys. Rev. E* **2015**, *92*, 050903.
- (19) Chowdhury, A.; Barbay, S.; Clerc, M. G.; Robert-Philip, I.; Braive, R. Phase Stochastic Resonance in a Forced Nanoelectromechanical Membrane. *Phys. Rev. Lett.* **2017**, *119*, 234101.
- (20) Dolleman, R. J.; Belardinelli, P.; Hourii, S.; van der Zant, H. S. J.; Alijani, F.; Steeneken, P. G. High-Frequency Stochastic Switching of Graphene Resonators Near Room Temperature. *Nano Letters* **2019**, *19*, 1282–1288.
- (21) Steele, G. A.; Hüttel, A. K.; Witkamp, B.; Poot, M.; Meerwaldt, H. B.; Kouwenhoven, L. P.; van der Zant, H. S. J. Strong Coupling Between Single-Electron Tunneling and Nanomechanical Motion. *Science* **2009**, *325*, 1103–1107.
- (22) Lassagne, B.; Tarakanov, Y.; Kinaret, J.; Garcia-Sanchez, D.; Bachtold, A. Coupling Mechanics to Charge Transport in Carbon Nanotube Mechanical Resonators. *Science* **2009**, *325*, 1107–1110.
- (23) Tabanera-Bravo, J.; Vigneau, F.; Monsel, J.; Aggarwal, K.; Bresque, L.; Fedele, F.; Cerisola, F.; Briggs, G. A. D.; Anders, J.; Auffèves, A.; Parrondo, J. M. R.; Ares, N. Stability of long-sustained oscillations induced by electron tunneling. *Phys. Rev. Res.* **2024**, *6*, 013291.

- (24) Usmani, O.; Blanter, Y. M.; Nazarov, Y. V. Strong feedback and current noise in nanoelectromechanical systems. *Phys. Rev. B* **2007**, *75*, 195312.
- (25) Wen, Y.; Ares, N.; Schupp, F. J.; Pei, T.; Briggs, G. A. D.; Laird, E. A. A Coherent Nanomechanical Oscillator Driven by Single-Electron Tunnelling. *Nat. Phys.* **2020**, *16*, 75–82.
- (26) Urgell, C.; Yang, W.; De Bonis, S. L.; Samanta, C.; Esplandiu, M. J.; Dong, Q.; Jin, Y.; Bachtold, A. Cooling and Self-Oscillation in a Nanotube Electromechanical Resonator. *Nat. Phys.* **2020**, *16*, 32–37.
- (27) Dellwo, D.; Keller, H. B.; Matkowsky, B. J.; Reiss, E. L. On the Birth of Isoloids. *SIAM J. Appl. Math.* **1982**, *42*, 956–963.
- (28) Moser, J.; Eichler, A.; Guettinger, J.; Dykman, M. I.; Bachtold, A. Nanotube Mechanical Resonators with Quality Factors of up to 5 Million. *Nat. Nanotech* **2014**, *9*, 1007–1011.
- (29) Zakharova, A.; Vadivasova, T.; Anishchenko, V.; Koseska, A.; Kurths, J. Stochastic bifurcations and coherence-like resonance in a self-sustained bistable noisy oscillator. *Phys. Rev. E* **2010**, *81*, 011106.
- (30) Nayfeh, A. H.; Balachandran, B. *Applied nonlinear dynamics: analytical, computational, and experimental methods*; John Wiley & Sons, 2008.
- (31) Willick, K.; Baugh, J. Self-driven oscillation in Coulomb blockaded suspended carbon nanotubes. *Phys. Rev. Res.* **2020**, *2*, 033040.
- (32) Weldon, J. A.; Alemán, B.; Sussman, A.; Gannett, W.; Zettl, A. K. Sustained Mechanical Self-Oscillations in Carbon Nanotubes. *Nano Letters* **2010**, *10*, 1728–1733.
- (33) Feng, X. L.; White, C. J.; Hajimiri, A.; Roukes, M. L. A self-sustaining ultrahigh-frequency nanoelectromechanical oscillator. *Nature Nanotechnology* **2008**, *3*, 342–346.

- (34) Sekaric, L.; Zalalutdinov, M.; Turner, S. W.; Zehnder, A. T.; Parpia, J. M.; Craighead, H. G. Nanomechanical resonant structures as tunable passive modulators of light. *Applied Physics Letters* **2002**, *80*, 3617–3619.
- (35) Zhang, P.; Jia, Y.; Yuan, S.; Liu, Z.; Yang, R. Tunable Stochastic State Switching in 2D MoS₂ Nanomechanical Resonators with Nonlinear Mode Coupling and Internal Resonance. *Nano Letters* **2024**, *24*, 11043–11050.
- (36) Benzi, R.; Sutera, A.; Vulpiani, A. The mechanism of stochastic resonance. *Journal of Physics A: Mathematical and General* **1981**, *14*, L453.
- (37) Nicolis, C. Stochastic aspects of climatic transitions—response to a periodic forcing. *Tellus* **1982**, *34*, 1–9.
- (38) Kramers, H. Brownian motion in a field of force and the diffusion model of chemical reactions. *Physica* **1940**, *7*, 284–304.
- (39) Dykman, M. I.; Golubev, G. P.; Luchinsky, D. G.; Velikovich, A. L.; Tsuprikov, S. V. Fluctuational transitions and related phenomena in a passive all-optical bistable system. *Phys. Rev. A* **1991**, *44*, 2439–2449.
- (40) Supporting Information.
- (41) Keşkekler, A.; Shoshani, O.; Lee, M.; van der Zant, H. S. J.; Steeneken, P. G.; Alijani, F. Tuning Nonlinear Damping in Graphene Nanoresonators by Parametric–Direct Internal Resonance. *Nat. Commun.* **2021**, *12*, 1099.
- (42) Singh, V.; Shevchuk, O.; Blanter, Ya. M.; Steele, G. A. Negative Nonlinear Damping of a Multilayer Graphene Mechanical Resonator. *Phys. Rev. B* **2016**, *93*, 245407.
- (43) Armour, A. D.; Blencowe, M. P.; Zhang, Y. Classical dynamics of a nanomechanical resonator coupled to a single-electron transistor. *Phys. Rev. B* **2004**, *69*, 125313.

- (44) Novotný, T.; Donarini, A.; Jauho, A.-P. Quantum Shuttle in Phase Space. *Phys. Rev. Lett.* **2003**, *90*, 256801.
- (45) Fedorets, D.; Gorelik, L. Y.; Shekhter, R. I.; Jonson, M. Quantum Shuttle Phenomena in a Nanoelectromechanical Single-Electron Transistor. *Phys. Rev. Lett.* **2004**, *92*, 166801.
- (46) Mozyrsky, D.; Hastings, M. B.; Martin, I. Intermittent polaron dynamics: Born-Oppenheimer approximation out of equilibrium. *Phys. Rev. B* **2006**, *73*, 035104.
- (47) Samanta, C.; De Bonis, S. L.; Møller, C. B.; Tormo-Queralt, R.; Yang, W.; Urgell, C.; Stamenic, B.; Thibeault, B.; Jin, Y.; Czaplewski, D. A.; Pistolesi, F.; Bachtold, A. Nonlinear nanomechanical resonators approaching the quantum ground state. *Nature Physics* **2023**, *19*, 1340–1344.
- (48) Minot, E. D.; Yaish, Y.; Sazonova, V.; Park, J.-Y.; Brink, M.; McEuen, P. L. Tuning Carbon Nanotube Band Gaps with Strain. *Phys. Rev. Lett.* **2003**, *90*, 156401.
- (49) Kagan, Y. Quantum diffusion in solids. *Journal of Low Temperature Physics* **1992**, *87*, 525–569.
- (50) Strogatz, S. *Nonlinear Dynamics and Chaos: With Applications to Physics, Biology, Chemistry, and Engineering*; Studies in Nonlinearity; Avalon Publishing, 2014.
- (51) Habib, G.; Cirillo, G. I.; Kerschen, G. Isolated resonances and nonlinear damping. *Nonlinear Dynamics* **2018**, *93*, 979–994.
- (52) Hill, T.; Neild, S.; Cammarano, A. An analytical approach for detecting isolated periodic solution branches in weakly nonlinear structures. *Journal of Sound and Vibration* **2016**, *379*, 150–165.
- (53) Cirillo, G.; Habib, G.; Kerschen, G.; Sepulchre, R. Analysis and design of nonlinear resonances via singularity theory. *Journal of Sound and Vibration* **2017**, *392*, 295–306.

- (54) Mélot, A.; Denimal Goy, E.; Renson, L. Control of isolated response curves through optimization of codimension-1 singularities. *Computers & Structures* **2024**, *299*, 107394.
- (55) Bureau, E.; Schilder, F.; Elmegård, M.; Santos, I. F.; Thomsen, J. J.; Starke, J. Experimental bifurcation analysis of an impact oscillator—Determining stability. *Journal of Sound and Vibration* **2014**, *333*, 5464–5474.
- (56) Gatti, G.; Brennan, M. J. Inner detached frequency response curves: an experimental study. *Journal of Sound and Vibration* **2017**, *396*, 246–254.
- (57) Detroux, T.; Noël, J.-P.; Virgin, L. N.; Kerschen, G. Experimental study of isolas in nonlinear systems featuring modal interactions. *PLOS ONE* **2018**, *13*, 1–25.
- (58) Dong, X.; Dykman, M. I.; Chan, H. B. Strong negative nonlinear friction from induced two-phonon processes in vibrational systems. *Nature Communications* **2018**, *9*, 3241.